Optimizing the flux coupling between a nanoSQUID and a magnetic particle using atomic force microscope nanolithography

M Faucher[1,3]**, P O Jubert**[1,2]**, O Fruchart**[1]**, W Wernsdorfer**[1] **and V Bouchiat**[1]

[1] Institut Néel, CNRS and Université J Fourier, BP 166, 38042 Grenoble Cedex 9, France
[2] IBM Almaden Research Center, CA, USA

Abstract
We present results of niobium based SQUID magnetometers for which the weak links are engineered by the local oxidation of thin films using an atomic force microscope (AFM). Firstly, we show that this technique allows the creation of variable thickness bridges with 10 nm lateral resolution. Precise control of the weak link milling is offered by the possibility to monitor, in real-time, the weak link conductance. Such a process is shown to enhance the magnetic field modulation and hence the sensitivity of the magnetometer. Secondly, AFM lithography is used to provide a precise alignment of nanoSQUID weak links with respect to a ferromagnetic iron dot. The magnetization switching of the near-field coupled particle is studied as a function of the applied magnetic field direction.

(Some figures in this article are in colour only in the electronic version)

1. Introduction

Atomic force microscope (AFM) lithography based on nano-oxidation of metallic thin films is a unique technique for the direct patterning of electronic devices at the nanometer scale [1]. The process involves the local surface oxidation of the metallic film under ambient conditions with a voltage-biased tip. Applied to ultrathin films, this allows the patterning of electrically-insulating oxide patterns (figure 1(a)) with a typically 10 nm nanometer linewidth. It has been used by Matsumoto *et al* [2] for the realization of nanoscale single electron devices showing room temperature operation [3, 4].

More recently the same technique has been applied to realize superconducting nanostructures [5] based on nanoscale constrictions, allowing the fabrication of niobium [5] and niobium nitride [6] nanoSQUIDs as well as single photon detectors [7]. Depending on the operating conditions (tip voltage bias and speed) and film thickness, oxidation of the film can be performed through part or all of the thickness (see figure 1(b)) of the entire film. The amount of metal transformed into the oxide can be indirectly determined by the measurement of the oxide protrusion. This interesting feature

---

[3] Present address: IEMN-Lille, Villeneuve d'Ascq, France.
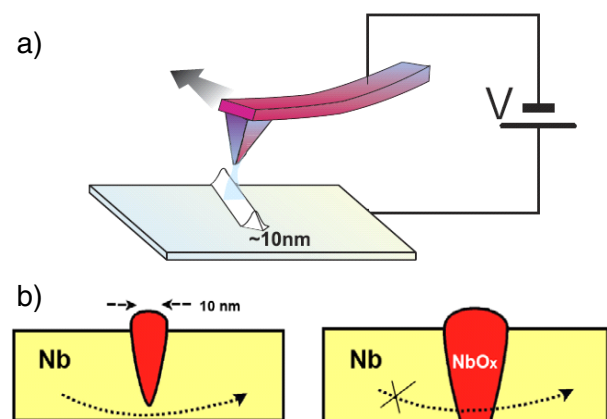
Figure 1. (a) Principle of AFM nanolithography by oxidation, (b) cross-section of an AFM produced oxide line drawn on a metallic ultrathin film. Depending on the oxidation parameters (tip bias, speed, humidity), oxidation of the film can be obtained in either a partial or the full thickness of the film.

allows a three-dimensional control of a superconducting nanostructure, similar to that which can be obtained using focused ion beam (FIB) milling [8–10]. Indeed AFM local oxidation has comparable resolution to that obtained using

FIB milling. It also benefits from some other advantages, such as the absence of contamination and the possibility to protect the nanostructure against further oxidation since the resulting nanostructure is embedded in the oxide generated by the anodization. Note, however, that unlike an FIB beam, which can penetrate thick samples, AFM oxidation is restricted to ultrathin films, as the oxidation can hardly be performed on thicknesses exceeding 10 nm. In this paper, we illustrate the versatility of this technique by extending its use to more complex structures. Here we describe two different experiments using AFM oxidation lithography to engineer the superconducting weak link and to optimize its operation. The first experiment involves the post-processing of a SQUID made by electron-beam lithography (EBL), while the second deals with the full fabrication of a nanoSQUID within multilayers made of ferromagnetic dots coated with superconducting niobium.

2. *In situ* milling of niobium nanoSQUID junctions using AFM oxidation

We first describe the AFM-based post-processing of microSQUID devices made by AFM oxidation on SQUID devices produced by EBL and plasma etching [11]. EBL allows the processing of a large number of devices with homogeneous geometrical factors, while AFM lithography allows one to refine the working characteristics of the bridges. On the tested sample, the two SQUID weak links are initially made of a lateral constriction of constant thickness (following the so-called 'Dayem' bridge [12] geometry). The SQUID is first imaged by the AFM without any tip bias to precisely align the tip over the Dayem bridge. The original size prior to AFM lithography consists of a nanowire of 60 nm width and 250 nm length. The AFM oxidation is then performed by proceeding to a single line scan perpendicular to the Dayem bridges (white arrow in inset of figure 2) and applying a voltage of about −10 V on the tip, with a relative humidity exceeding 50%. The effect of the oxidation can be monitored either directly by measuring in real-time the nano-bridge resistance increase (the two terminal resistance increases by typically a few percent) or by imaging the oxide protrusion during a subsequent AFM scan without an applied voltage (see figure 2). Indeed, the oxidation process results in a swelling of the bridge under the tip trajectory. Under repeated scans using low scan speeds ($\sim$0.1 μm s^{-1}), the oxidation is homogeneously done below the tip trajectory resulting in an even swelling (figure 2 top). If the tip scan speed is increased in the range of 1–3 μm s^{-1}, the oxidation only occurs on the bridge edges, as evidenced by the observation of the oxide protrusion only on the bridge sides (see figure 2, bottom). This selectivity effect is attributed to the stronger interaction of the wire edge with the biased AFM tip. In order to illustrate the power of AFM oxidation, we selected a sample which exhibits a rather poor magnetic flux modulation of switching current I_{sw} before processing (black curve of figure 3). We have tested the effect of the oxidation procedure by measuring the magnetic field modulation at low temperature of the same SQUID before and after the oxidation step
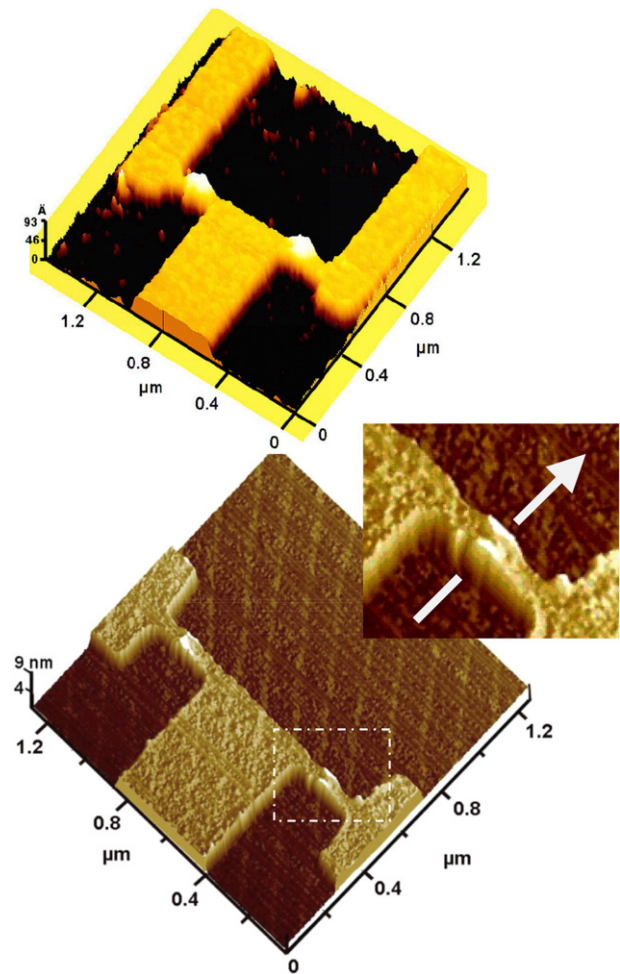
Figure 2. AFM micrographs of SQUID weak links made of Dayem bridges partially oxidized using AFM lithography. (Top) Using a low scan speed of the tip: the weak link section is homogeneously reduced. (Bottom) Using a high scan speed of the tip: only the edges of the weak links are oxidized (see zoom in inset). The white arrow indicates the tip motion during lithography.

(figure 3, black and blue curves, respectively). The first observation is that the maximum switching current of the trimmed SQUID is reduced by roughly a factor 2 due to the decreased cross-section of the weak links. However, it exhibits a much better magnetic flux (figure 3) dependence with a typical sawtooth-shaped modulation. This last effect can be understood as a consequence of the change in the local topology in the weak links resulting from the oxidation. The SQUID interference contrast in a SQUID with 'long' Dayem bridges (i.e. where bridge lengths are longer than the superconducting coherence length) is known to be inversely proportional to the kinetic inductance [13] of the bridge, the latter being directly proportional to L/S [14], where L and S are respectively the length and the cross-section of the weak link [6]. The effect of the oxidation is to locally decrease S (say by a factor 2) on a lateral size L' of the order of the lateral size of the patterned oxide line (around 10 nm) [5], which is much smaller than L. One thus transforms the effective weak link from the class of constant thickness ('Dayem') bridges [12] towards the class of 'variable thickness bridges (VTB)', [13]. Furthermore, in VTB
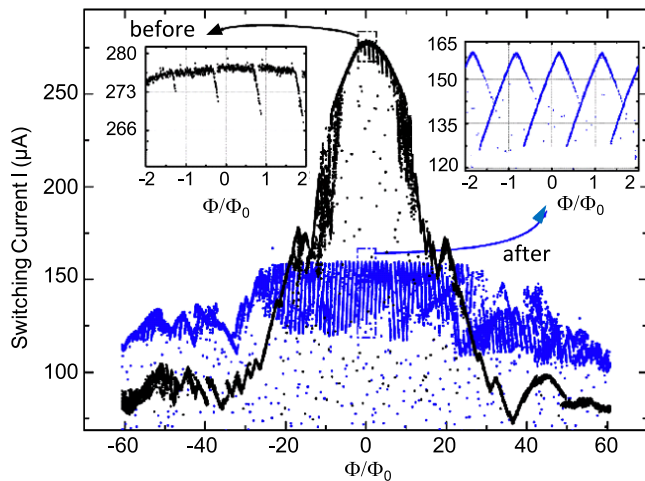
Figure 3. Measurement of the switching current at 30 mK of the nanoSQUID as a function of the applied magnetic field (shown in reduced units of flux quanta) before (data labeled 'before' (black dots in the online version)) and after (data labeled 'after' (blue dots in the online version)) AFM oxidation of the nano-bridges.

based SQUID, the torsion of the phase induced by the circulating current through the weak link is more localized compared to devices with Dayem bridge weak links [15]. Note that at magnetic field values $|B| > 25\Phi_0$, the current of the VTB SQUID exceeds the Dayem SQUID and the two modulation curves intersect each other. Indeed a smaller weak link is less sensitive to the penetration of the magnetic field. Therefore, shrinking the weak link size results in widening the envelope of the modulation curve (known as a Fraunhofer pattern). At higher fields, where the SQUID is no longer periodically modulating, the switching current exhibits similar variations before and after AFM oxidation: for example, the variations recorded between -60 and $-40\Phi_0$ show a clear correlation. In other cases (i.e. 30–$60\Phi_0$) such a similar correlation can still be seen but the VTB SQUID show remnant periodic oscillations superimposed on that signal. The unmodulated component presumably comes from depinning of vortices in the superconducting stripes away from the weak links. Since these parts are not affected by the AFM lithography step, their behaviors are unchanged by the weak link engineering.

3. AFM made nanoSQUIDs coupled to a single self-assembled nanoscale iron dot

The second experiment illustrates the potential of AFM nano-oxidation as a stand-alone fabrication technique. For that purpose, we use the oxidation process on a plain multilayer substrate to pattern a nanoSQUID as a final fabrication step. This order allows us to accurately position the detector with respect to the probed magnetic object, thus optimizing flux pick-up.

The chosen substrate is a superconducting/ferromagnetic multilayer where a nanoSQUID junction must be coupled to a single nanomagnet. Indeed it has been shown [16, 17] that the best inductive coupling of a nanomagnet to a nanoSQUID is achieved when the magnet is in direct proximity to one
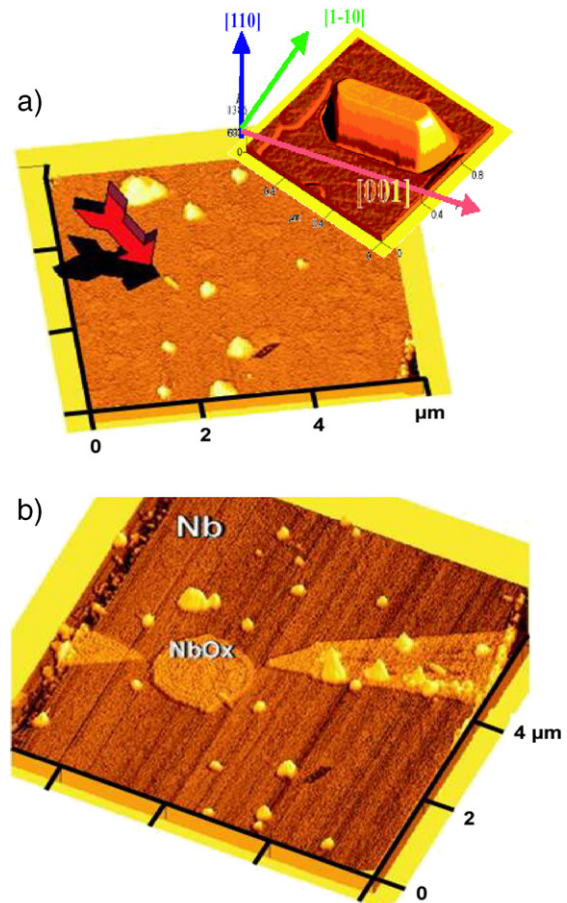
Figure 4. (a) AFM micrograph of the multilayered sample before the lithography step. The arrow indicates the ferromagnetic particle chosen to be coupled to the nanoSQUID magnetometer. Inset: zoomed AFM micrograph of an iron magnet showing the faceted structure of the submicron ingot. (b) AFM micrograph of the same sample after the AFM patterning of the oxide nanostructures. It is composed of three features: a central disc which acts as the SQUID loop and two lateral wedges. The two wedge-disk gaps define the Dayem constrictions which will be the sensing parts of the magnetometer.

of the junctions. The magnet chosen for this experiment is a sub-micrometer sized faceted iron dot, which exhibits high structural quality and displays simple magnetic flux-closure states. These dots are self-assembled and then encapsulated under a protective capping layer in an ultra-high vacuum using pulsed-laser epitaxy [18]. They are grown on a sapphire substrate of orientation ($11\bar{2}0$) initially buffered *in situ* with an 8 nm-thick molybdenum film, which provides the necessary conditions to give rise to self-assembly. Note that besides the predominant iron dot growth, there exist other sorts of bi-dimensional nanostructure attributed to an iron–molybdenum surface alloy (which can be seen in figure 4(a) and are labeled 'Fe-2D') partially wetting the molybdenum film. A capping layer made of a trilayer of oxidized aluminum (2 nm) followed by niobium (15 nm) and then silicon (2 nm) is evaporated. Each film of the capping layer has a given purpose. The niobium layer provides the source of superconductivity and is protected from contamination and oxidation by both the
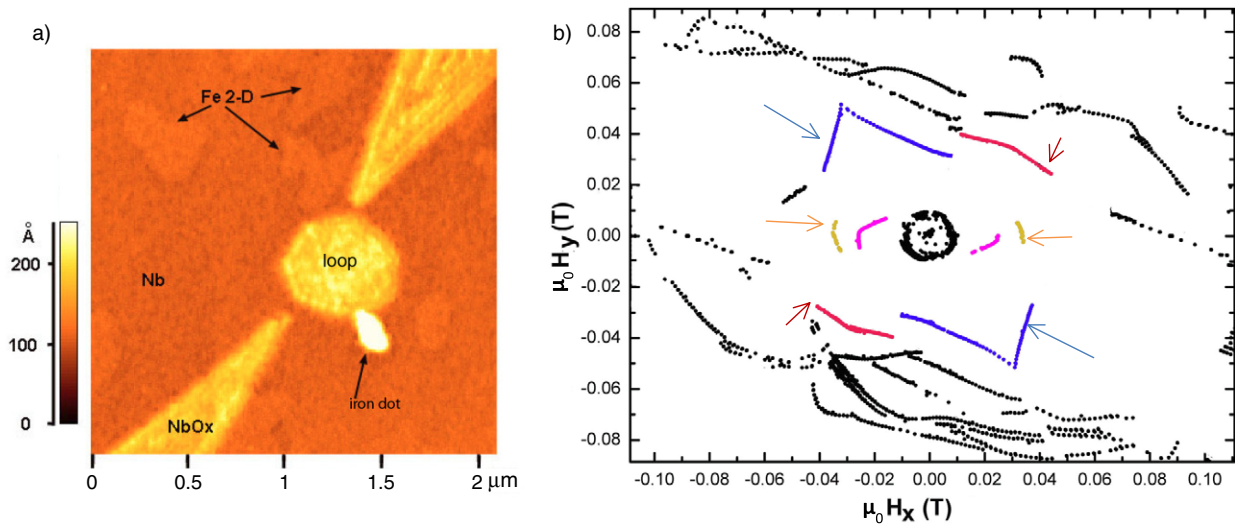
Figure 5. Left: AFM micrograph of the test sample showing the alignment of the patterned SQUID with respect to a single iron dot surrounded by the patterned SQUID. Right: polar map of the switching field, measured for the AFM nanoSQUID depicted on the left, as a function of the field amplitude (H_x, H_y). Curves symmetrically highlighted by arrows (colored in the online version) emphasize the portions of Stoner–Wohlfarth astroids, each of them being the signature of magnetization switching events.

under and over layers. The aluminum oxide buffer layer intercalated between the iron particle and the niobium is effective in reducing the inverse proximity effect that plagues superconducting thin films in close contact with ferromagnetic materials.

Since the dot formation results from a self-assembly process, its position on the film is not controlled. This implies that the nanoSQUID junction has to be precisely aligned with respect to the magnetic particle to be measured. The ease of alignment provided by scanning probe microscopy offers a good opportunity to precisely align a given nanostructure with respect to another nano-object. In previous experiments, [19], alignment was obtained statistically by selecting 'good' devices among a large ensemble of batch-processed samples. The present technique offers the advantage of allowing work on prototypes only existing as single samples. Alignment of the AFM tip prior to the oxidation patterning step can be performed with an extremely good accuracy (precision better than 10 nm) if one uses an atomic force microscope equipped with piezoelectric actuators corrected for their non-linearity (so-called 'closed-loop scanner'). One should note the film is not altered during this alignment procedure since imaging is performed in the absence of a voltage applied on the tip.

We have selected an Fe dot of size 200 nm × 50 nm × 30 nm (figure 5(a)). Both SQUID loop and lateral constrictions are made of fully oxidized patterned lines using the conditions described in [5]. The low density allows the study of a single dot coupled to a nanoSQUID magnetometer. The resulting structure is presented in figure 4(b). It consists of a circular oxide circle and two lateral oxide wedges defining 40 nm wide Dayem constrictions. A minimal distance of 400 nm is maintained between the magnet and the oxide loop in order to protect the ferromagnetic particle from the oxygen diffusion induced by the AFM lithography (figure 5, left). The sample is then transferred to a dilution fridge

equipped with 3D superconducting coils which allow the study of magnetization reversal properties below 40 mK, as similarly performed in [20–22].

The typical distances between dots are such that the magnetostatic interactions between them can be neglected, so that they behave essentially like isolated nanomagnets. These have been shown experimentally, by magnetic force microscopy and by micromagnetic simulation, to display flux-closure magnetic domains [23]. This can be understood as Fe is a rather soft magnetic material. Micromagnetic simulations later predicted the magnetization processes under a field of such dots: starting from saturation, upon reducing the external field one or several magnetic vortices or domain walls enter the dot at its edges (nucleation events), yielding the flux-closure state at remanence. Upon again increasing the external field the magnetic vortices and domain walls are expelled at an edge (annihilation events). It is the fields, at which the nucleation or annihilation events occur, that the microSQUID will detect in the so-called 'cold-mode' [14, 21]. The magnetization process of these dots has been simulated in detail and microSQUID measurements were obtained in [19] confirming a multi-domain structure with a clear angular dependence of the magnetization. This magnetization depends on both intrinsic (shape, anisotropy) and extrinsic (microstructure, defects) parameters. The dots (see the AFM micrograph in figure 4(a), inset) have an elongated hexagonal shape and exhibit atomically flat facets. The magnetic field is applied within the plane of the SQUID and ramped from zero to a maximum amplitude of about 0.3 T at a given and fixed azimuth angle. This azimuth angle is varied between scans through a given step in order to cover the whole x–y-plane, while feedback is applied in the z-direction to keep the SQUID at the same working point (i.e. a constant switching current). Flux jumps are recorded, analyzed, and then plotted in the x–y-plane. Figure 5 (right)

shows the plots of the switching values of the nanoSQUID recorded at in the *cold-mode* method [14, 21], here performed at 40 mK. The jumps may come from various origins: the sought signal, i.e. jumps associated to nucleation/annihilation events in the 3D Fe dots, and parasitic signals, including the magnetization reversal of the 2D Fe platelets or the motion of unpinned vortices within the Nb. In this plot, one can highlight four colored branches exhibiting a point symmetry with respect to the origin, whose shapes are portions of a 3D geometrical astroid [24]. Such an individual shape is similar to the model proposed by Stoner and Wohlfarth [25] to describe single-domain magnetization reversal. Entangled astroids have already been observed in other microSQUID experiments where the microSQUID had been patterned with a regular EBL technology. This feature is expected in the case of flux-closure dots, where several nucleation/annihilation events may be expected to turn a single-domain state into a flux-closure state, and vice versa [19].

4. Conclusion

These two series of experiments bring an insight into the potential of scanning probe nanolithography for optimizing the operation of a nanoSQUID interferometer. The simplicity and precision of alignment and the possibility of easy *in situ* control of the device geometrical and electrical parameters are unique features associated with this technique. We have shown that this type of lithography allows an increase in magnetometer sensitivity in the near-field regime by optimizing two independent parameters. Firstly, the miniaturization of the weak links increase the magnetometer responsivity, and secondly, the ease of the alignment offers new possibilities to increase the near-field inductive coupling between the magnetometer and the magnetic elements to be studied.

Acknowledgment

References

[1] Snow E S and Campbell P M 1995 *Science* **270** 1639–41
[2] Matsumoto K, Ishii M, Segawa K, Oka Y, Vartanian B J and Harris J S 1996 *Appl. Phys. Lett.* **68** 34
[3] Shirakashi J-I, Matsumoto K, Miura N and Konagai M 1998 *Appl. Phys. Lett.* **72** 1893–5
[4] Matsumoto K, Gotoh Y, Maeda T, Dagata J A and Harris J S 2000 *Appl. Phys. Lett.* **76** 239–41
[5] Bouchiat V, Faucher M, Thirion C, Wernsdorfer W, Fournier T and Pannetier B 2001 *Appl. Phys. Lett.* **79** 123–5
[6] Faucher M, Fournier T, Pannetier B, Thirion C, Wernsdorfer W, Villegier J C and Bouchiat V 2002 *Physica* C **368** 211
[7] Delacour C *et al* 2007 *Appl. Phys. Lett.* **90** 191116
[8] Tettamanzi G C, Pakes C I, Potenza A, Marrows C H, Prawer S and Jamieson D N 2006 *30th Annual Condensed Matter and Materials Mtg (Australia)*
[9] Troeman A G P, Derking H, Borger B, Pleikies J, Veldhuis D and Hilgenkamp H 2007 *Nano Lett.* **7** 2152–6
[10] Hao L, Macfarlane J C, Gallop J C, Cox D, Beyer J, Drung D and Schurig T 2008 *Appl. Phys. Lett.* **92** 192507
[11] Mailly D, Chapelier C and Benoit A 1993 *Phys. Rev. Lett.* **70** 2020
[12] Anderson P W and Dayem A H 1964 *Phys. Rev. Lett.* **13** 195
[13] Likharev K K 1979 *Rev. Mod. Phys.* **51** 101
[14] Meservey R and Tedrow P M 1969 *J. Appl. Phys.* **40** 2028
[15] Hasselbach K, Mailly D and Kirtley J R 2002 *J. Appl. Phys.* **91** 4432
[16] Wernsdorfer W 1996 *PhD Thesis* J Fourier University, Grenoble
[17] Bouchiat V 2009 *Supercond. Sci. Technol.* **22** 064002
[18] Jubert P O, Fruchart O and Meyer C 2001 *Phys. Rev.* B **64** 115419
[19] Fruchart O, Toussaint J C, Jubert P O, Wernsdorfer W, Hertel R, Kirschner J and Mailly D 2004 *Phys. Rev.* B **70** 172409
[20] Wernsdorfer W, Hasselbach K, Mailly D, Barbara B, Benoit A, Thomas L and Suran G 1995 *J. Magn. Magn. Mater.* **145** 33
[21] Wernsdorfer W, Bonet-Orozco E, Hasselbach K, Benoit A, Barbara B, Demoncy N, Loiseau A, Pascard H and Mailly D 1997 *Phys. Rev. Lett.* **78** 1791
[22] Fruchart O, Wernsdorfer W, Nozières J P, Givord D, Rousseaux F, Mailly D, Decanini D and Carcenac F 1999 *J. Magn. Magn. Mater.* **198/199** 228–30
[23] Jubert P-O, Toussaint J-C, Fruchart O, Meyer C and Samson Y 2003 *Europhys. Lett.* **63** 132
[24] Slonczewski J C 1956 *Research Memo RM 003.111.224* IBM Research Center, Poughkeepsie, NY
[25] Stoner E C and Wohlfarth E P 1948 *Phil. Trans. R. Soc.* A **240** 599